Biological, Medical Devices, and Systems

Absolute Blood Pressure Waveform Monitoring Using an Ultrasound Probe

A. Chandrasekhar, A. Aguirre, H.-S. Lee, C. G. Sodini
Sponsorship: MEDRC-Philips, Analog Devices Inc., CICS

Accurate measurement of the absolute blood pressure (ABP) waveform assists clinical decision-making as it helps physicians titrate the cardiovascular therapy for a patient. In an intensive care unit (ICU), physicians use an invasive radial catheter to measure BP, whereas, outside an ICU, one may resort to isolated spot measurement of the BP via a brachial arm cuff device. These cuff devices measure only the systolic and diastolic values of the BP waveform, and unlike an arterial catheter used in an ICU, they do not output the shape of the ABP waveform. Morphology of the ABP waveform is significant as it reflects the hemodynamics of the underlying vasculature, and hence there is a need for a non-invasive and easy-to-use device that can output the ABP waveform. Ultrasound-based devices are a feasible alternative for monitoring the BP waveform as these devices can accurately measure pressure-dependent parameters like the blood flow velocity and arterial diameter waveforms. In this project, we are developing an algorithm (see Figure 1) to convert ultrasound data into an ABP waveform, and in this report, we present the preliminary results on estimating pulse pressure (PP) from the ultrasound data.

Two studies were performed to investigate the proposed PP estimation algorithm (See Algorithm Stage 1 in Fig. 1). In study 1, signals illustrated in Figure 1 were recorded from the carotid artery using a custom-designed ultrasound probe while the subject was supine, whereas, in study 2, the above-mentioned signals were recorded using a Philips ultrasound-transducer (XL-143) while the subject rested supine and in tilted posture. Gold standard PP was measured from the brachial artery using an Omron BP monitor as a reference. The Bland-Altman plot in Figure 2 shows that the estimated PP can track the gold standard PP values.

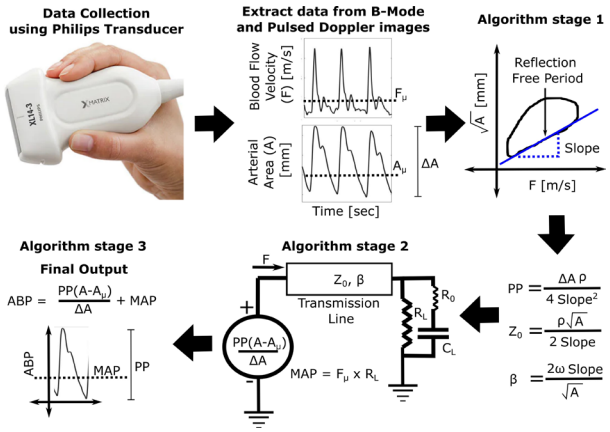

▲ Figure 1: Step by step algorithm to estimate pulse pressure and ABP waveform from ultrasound signals.

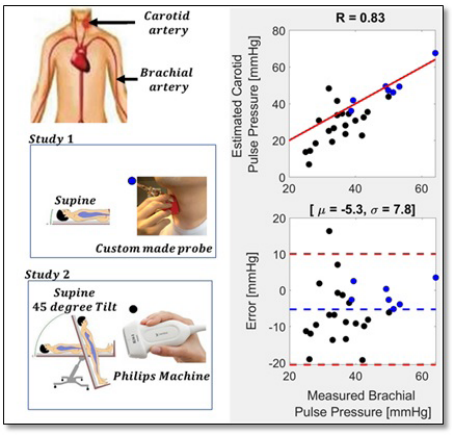

▲ Figure 2: Pulse pressure estimated via ultrasound signals recorded at the carotid artery.

FURTHER READING

- J. Seo, "A Non-invasive Central Arterial Pressure Waveform Estimation System Using Ultrasonography for Real-time Monitoring," Dissertation, Massachusetts Institute of Technology, Cambridge, 2018.

An Implantable Soft Robotic Platform for Enhanced Drug Delivery

D. Goswami, W. Whyte, S. X. Wang, Y. Fan, N. A. Ward, G. P. Duffy, E. B. Dolan, E. T. Roche
Sponsorship: Juvenile Diabetes Research Foundation

Fibrous capsule formation, and its effect on molecular transport, can be detrimental to the long-term efficacy of implantable drug delivery devices, especially when precise spatial and temporal control is necessary for safe and effective therapy delivery. We report an implantable platform which can overcome the diffusional barrier of the fibrous capsule to achieve enhanced transport of small and macromolecular therapy using multiple synergistic soft robotic strategies (Figure 1a, b). Using this platform, small amplitude dynamic actuation (preconditioning) applied to subcutaneous tissue in mice leads to a downstream functional effect: enhanced passive transport of insulin (a model macromolecule) and glycemic control (Figure 1c). Furthermore, rapid actuation of the platform at the time of drug delivery can accelerate transport via convective fluid flow and overcome diffusional limitations caused by the fibrous capsule (Figure 2). This soft actuatable platform has potential clinical utility for mediating and overcoming the host fibrotic response, leading to enhanced delivery of drug therapy for a variety of indications.

The management of type 1 diabetes is one relevant clinical area where our platform could provide synergistic benefit. For example, dynamic actuation could be applied to extend the lifespan of an artificial pancreas, preventing unnecessary fibrous capsule mediated blockages, linked hyperglycemic events, and ultimately simplifying the dosing regimen and patient experience. In synergy, actuation at the time of drug delivery could make rapid insulin adjustments and maintain blood glucose levels in the narrow window necessary to prevent long-term complications. Looking further into the future, application of this platform could enable translation of next-generation bioartificial technologies utilizing human-derived insulin-producing islet cells by modifying the transport-limiting fibrous capsule, which has been a major barrier to the viability of cell-based therapeutics.

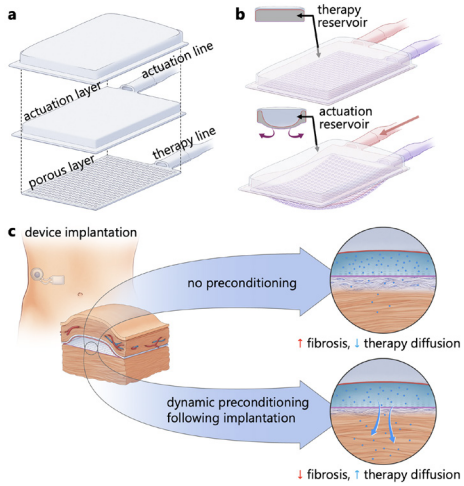

▲Figure 1: a) Exploded view showing the different layers comprising the implantable soft robotic platform. b) Deflection of the actuation and porous layers during actuation. c) Overview of device functionality during dynamic actuation.

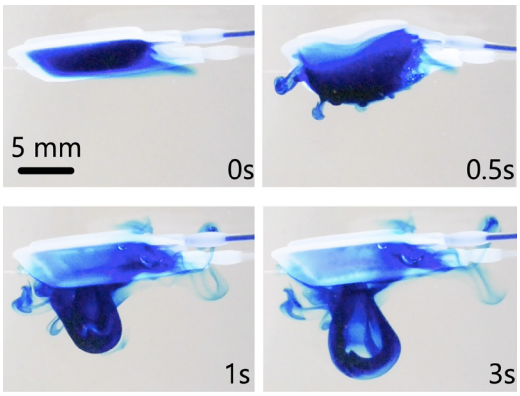

▲Figure 2: Rapid actuation at the time of drug delivery enables convective flow of a model drug, methylene blue, from the therapeutic reservoir of the device.

FURTHER READING

- D. Goswami, D. A. Domingo-Lopez, N. A. Ward, J. R. Millman, G. P. Duffy, E. B. Dolan, and E. T. Roche, "Design Considerations for Macroencapsulation Devices for Stem Cell Derived Islets for the Treatment of Type 1 Diabetes," *Advanced Science*, vol. 8, no. 16, p. 2100820, Jun. 2021.
- E. B. Dolan, C. E. Varela, K. Mendez, W. Whyte, R. E. Levey, S. T. Robinson, E. Maye, J. O'Dwyer, R. Beatty, A. Rothman, Y. Fan, J. Hochstein, S. E. Rothenbucher, R. Wylie, J. R. Starr, M. Monaghan, P. Dockery, G. P. Duffy, and E. T. Roche, "An Actuatable Soft Reservoir Modulates Host Foreign Body Response," *Science Robotics*, vol. 4, no. 33, pp. eaax7043, Aug. 2019.

Modeling the Arterial System to Improve Ultrasound Measurements of Hemodynamic Parameters

J. Harabedian, A. Chandrasekhar, C. G. Sodini
Sponsorship: Analog Devices

One of the most crucial parameters for monitoring cardiovascular disease risk is one's arterial blood pressure (ABP). Clinicians use a radial arterial catheter to measure ABP in an intensive care unit (ICU). Although this method is considered the gold standard, its invasive nature makes it undesirable and inaccessible outside an ICU. One solution to this problem is to take advantage of ultrasonic measurements, which are noninvasive and extremely accessible. However, developing an algorithm to convert ultrasound data into a legitimate ABP waveform requires an extensive amount of patient data. The limitation is that this data is difficult to obtain and impossible to fully control.

The solution presented here is to use a flow phantom: a physical, hydraulic system that mimics arterial blood flow. The phantom provides pressure waveforms, which come directly from a catheterized tube, and flow velocity waveforms, from an ultrasonic flow meter, that closely match the morphology of patient data. Developing a physical model of the arterial system allows for control of parameters that are considered uncontrollable in humans (e.g., arterial compliance, cardiac output, critical closing pressure) and enables data collection for a number of parameter combinations that would otherwise be unobtainable.

A flow phantom can be made using a pump, accumulator, compliant tubing, flow control valve, and a reservoir, representing the heart, large arterial compliance, large artery, arteriole resistance, and the ground pressure, respectively. To collect data from the phantom there are two pressure transducers, a flowmeter and the ultrasound device. Figure 1 shows the setup of the entire system. The pressure transducers and the flowmeter can collect control measurements that can be tested against the ultrasound device and the developed ABP estimation algorithm. Figure 2 shows example outputs from these measurement devices.

Experimental validation shows that the flow phantom does in fact mimic the hemodynamic behavior of arterial blood flow. This was confirmed by controlling various parameters of the system (e.g., flow resistance, ground pressure, cardiac output) and comparing its response against known hemodynamic responses.

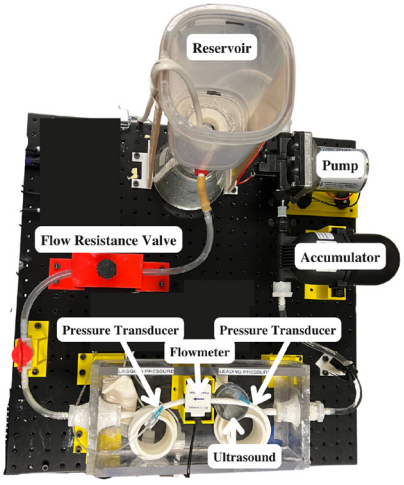

▲ Figure 1: Physical flow phantom system, consisting of the pump, accumulator, compliant tubing, flow control valve and reservoir. There are also the measure-ment devices: two pressure transducers, one flowmeter and in-house ultrasound device.

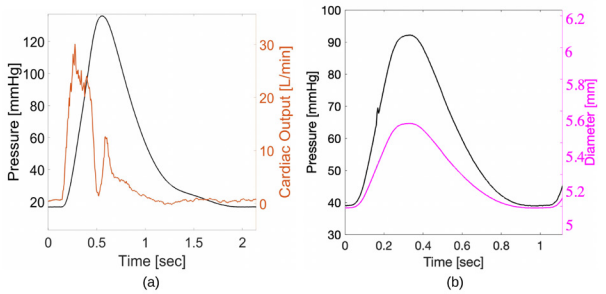

▲ Figure 2: Examples of typical measurements from flow phantom. 2a shows pressure and volumetric flow, with .5 Hz heart beat and pump on for .3 seconds. 2b shows pressure and diameter, with 1 Hz heartbeat and pump on for .2 seconds.

Model-based Noninvasive Intracranial Compliance and Vascular Resistance Estimation

S. M. Imaduddin, C. G. Sodini, T. Heldt
Sponsorship: Analog Devices, Inc. via MIT Medical Electronic Device Realization Center

Existing neuromonitoring methods used for patients with severe head injury tend to be highly invasive and carry a risk of tissue damage and infection. In particular, fluid infusion/withdrawal studies via indwelling catheters are needed to determine intracranial compliance (ICC) – an index of the propensity of rise in intracranial pressure (ICP) in response to changes in cranio-spinal volume. Despite their potential to serve as early indicators of intracranial hypertension, ICC measurements are rarely performed owing to time-consuming, invasive measurement protocols. In addition, measurements of cerebrovascular resistance (CVR) to blood flow are useful in assessing cerebral autoregulation and tracking pathological vascular narrowing such as in moyamoya disease. Like ICC, however, CVR is not regularly obtained at the bedside as the requisite measurements – arterial blood pressure (ABP), cerebral arterial blood flow (CBF), and ICP – are rarely monitored simultaneously.

We previously developed a noninvasive, model-based approach for ICP estimation. Recently, we augmented our approach to additionally estimate ICC and CVR. In particular, subjects' ABP and CBF are related to the ICP, ICC, and CVR via a Windkessel-like model. Measurements of the ABP and CBF are then used to estimate the clinically interpretable model parameters in a noninvasive, patient-specific fashion. Ultrasound-based CBF measurements were made in extracranial (common/internal carotid) arteries. Vessel diameters were estimated with B-mode images and combined with color flow velocity measurements to yield the CBF. Tilt-table studies were carried out to validate the proposed method. We found that our system successfully tracked tilt-induced changes in ICP, ICC, and CVR, paving the way towards convenient and safe neuromonitoring across a wide spectrum of pathologies, patient ages, and disease severities.

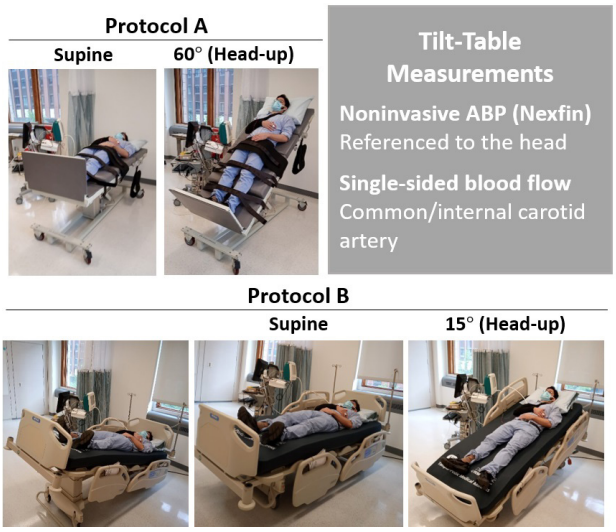

▲ Figure 1: Illustration of tilt-table protocols for method validation. Two protocols were established. Protocol A involved transitions from supine to 60° head-up position. Protocol B involved both head-up and head-down transitions of 15°, respectively. Acquired measurements are also listed.Closed electronics box with force and accelerometer analog inputs from the casing and data streaming to a tablet for data collection and display. Bottom: Electronics box components consisting of the DC power source of two series 9V batteries, the force signal amplifier, and the multi-channel analog-to-digital converter.

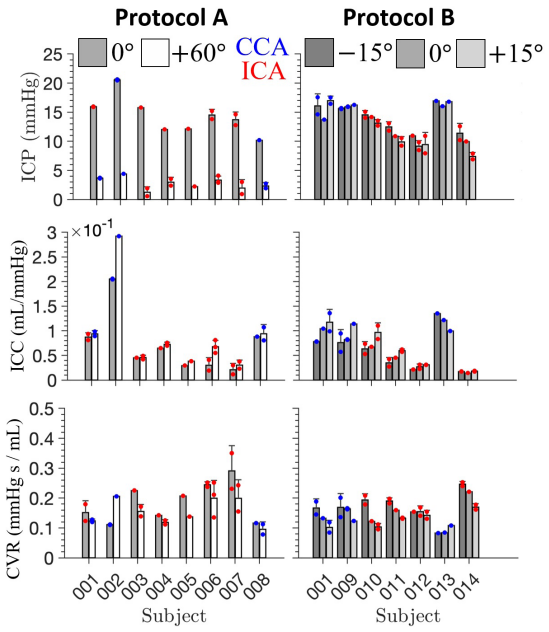

▲ Figure 2: Parameter estimation summary. Results obtained with recordings at common carotid (CCA) and internal carotid (ICA) arteries are shown in blue and red, respectively. ICP estimates decreased as subjects progressively moved to head-up positions. ICC estimates increased while CVR estimates decreased on average.

Venous Pressure Waveform Generation with Force-coupled Ultrasound

A. Jaffe, B. Anthony
Sponsorship: Medical Electronic Device Research Center-Philips

Congestive heart failure is diagnosed in 6.2 million people and is on 380,000 death certificates annually in the United States alone. In this syndrome, the heart's pumping ability decreases, causing the circulatory system to compensate by increasing blood volume to make blood easier to pump. Decompensated heart failure occurs when this mechanism is no longer effective, causing a vicious cycle of increasing volume, leading to pulmonary and peripheral edema from high venous pressure, which can lead to death. Currently, accurate venous pressure can be obtained only through invasive catheterization. In our project, we aim to mirror this accuracy in a noninvasive force-coupled ultrasound approach.

In our methodology, we acquire and segment force-coupled ultrasound images of the internal jugular vein (IJV) compression and note how much force is required to completely occlude it–the collapse force. We use the collapse force and IJV area at constant force to inform a 3-D inverse finite element model that produces a venous pressure waveform. We note that the pulsation of the nearby carotid artery compresses the IJV during systole and allows the IJV to expand during diastole. Given we have validated our methodology with the current noninvasive standard at MIT, we now begin a study using the invasive catheterization at Massachusetts General Hospital.

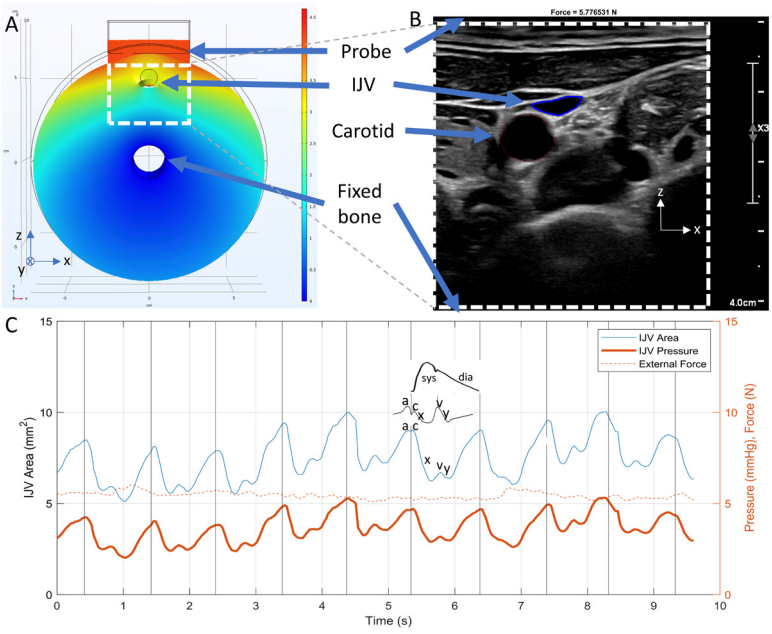

▲Figure 1: (A) Front-view of the 3-D finite element forward model of a force-coupled ultrasound compression of the IJV. (B) Force-coupled ultrasound image of the IJV and carotid short-axis cross-sections at the base of the neck. (C) Inverse finite element model inputs (IJV area and external force) and output (IJV pressure). Components of the venous pressure waveform are labeled (a, c, x, v, and y) and compared to an idealized venous pressure waveform. Vertical lines symbolize end-diastole; an idealized carotid pressure waveform is shown between two vertical lines.

Spiral Inertial Microfluidic System for Membrane-Free Cell Retention with Industrial-scale Cell-density Capacity and Throughput in Biomanufacturing

H. Jeon, T. Kwon, J. Han
Sponsorship: NIIMBL

Therapeutic proteins (e.g., monoclonal antibodies) are secreted from engineered host cells, and their separation from the host cells is essential to harvest purified proteins while the host cells continuously keep producing the therapeutic proteins in a bioreactor. Membrane-based filtration is the most widely used separation method for the biomanufacturing process. Although the method has a great separation efficiency, it has critical issues with membrane fouling and low product recovery due to nonspecific binding to the membrane surface.

To overcome these limitations, we developed and advanced spiral inertial microfluidic system for membrane-free cell retention with the following two key aims: 1) high cell-density capacity and 2) high throughput. For the first aim, elasto-inertial microfluidics was developed to manipulate ultra-high-density cells to achieve stable equilibrium positions in microchannels, aided by the inherent viscoelasticity of high-density cell suspension (Figure 1a, b). Using the cascaded configuration of two spiral devices in series, Chinese hHamster oOvary (CHO) cell retention was demonstrated, from 29.7 PCV% (108.1 million cells/mL) to 8.3 PCV% (33.2 million cells/mL) with overall 72.1% reduction efficiency (Figure 1c). For the second aim, based on channel deformation analysis aided by numerical simulation and confocal imaging, the empirically optimized design of a polydimethylsiloxane (PDMS) device for CHO cell retention was translated to its plastic equivalent. As shown in Figure 1d, the developed plastic device showed great performance on CHO cell retention with a high cell-removal rate (up to 97% at the input CHO cell density of ~12 million cells/mL). Furthermore, withby a simple stacking method, a multiplexed plastic device can be fabricated for high-throughput applications. Using the multiplexed plastic unit, we successfully demonstrated continuous, clogging-free, and ultra-high-throughput (at a processing rate of 1 L/min) cell clarification with a high cell-retention efficiency (Figure 1e, f), which can meet the throughput required for the large-scale industrial biomanufacturing applications.

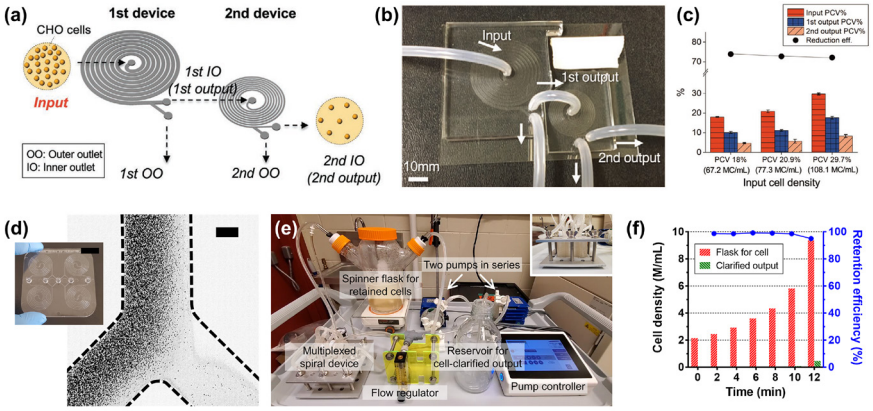

▲ Figure 1: (a) A schematic diagram and (b) an actual photo of two spiral devices in cascaded configuration to process ultra-high cell-density suspension. (c) Density reduction at three different input cell densities using the cascaded configuration. (d) Trajectory of CHO cells at the outlet bifurcation region of the plastic spiral device wiat the flow rate of 40 mL/min (scale bar: 500 μm); the inset represents a photo of the plastic device (scale bar: 20 mm). (e) A photo of the high-throughput cell-clarification platform using a 25-layers-stacked device (inset). (f) Profiles of the cell densities in the flask of the retained CHO cells (red bar), and the cell-clarified output (green bar), and the cell-retention efficiency (blue line) (input volume: ~ 1 L, input flow rate: 1 L/min, flow rate division: 15:1=the inner wall side output: the outer wall side output).

FURTHER READING

- H. Jeon, T. Kwon, J. Yoon, and J. Han, "Engineering a Deformation-free Plastic Spiral Inertial Microfluidic System for CHO Cell Clarification in Biomanufacturing,", *Lab on a Chip*, Vol. 22, no. (2), p. 272, (2022), DOI: 10.1039/D1LC00995H.
- T. Kwon, K. Choi, and J. Han, "Separation of Ultra-High-Density Cell Suspension via Elasto-Inertial Microfluidics,", *Small*, vol. Vol. 17, no. (39), p. 2101880, (2021), DOI: 10.1002/smll.202101880.
- H. Jeon, T. Kwon, J. Yoon, and J. Han, "Biomanufacturing Scale CHO Cell Clarification Using Hard Plastic Spiral Inertial Microfluidic Device,", *presented at MicroTAS 2021*, , In-person & Virtual, Palm Springs, CA, USA (Oct. 10–14, 2021).

Functional Drug Susceptibility Testing Using Single-cell Mass Predicts Treatment Outcome in Patient-derived Cancer Spheroid Models

M. A. Stockslager, S. Malinowski, M. Touat, J. C. Yoon, J. Geduldig, M. Mirza, A. S. Kim, P. Y. Wen, K. H. Chow, K. L. Ligon, S. R. Manalis

Sponsorship: Koch Institute Center for Precision Cancer Medicine, Dana Farber Cancer Institute Center for Patient Derived Models

Functional precision medicine aims to match individual cancer patients to optimal treatment through ex vivo drug susceptibility testing on patient-derived cells. However, few functional diagnostic assays have been validated against patient outcomes at scale because of the limitations of such assays. Here, we describe a high-throughput assay that detects subtle changes in the mass of individual drug-treated cancer cells as a surrogate biomarker for patient treatment response. To validate this approach, we determined ex vivo response to temozolomide in a retrospective cohort of 69 glioblastoma patient-derived neurosphere models with matched patient survival and genomics. Temozolomide-induced changes in cell mass distributions predict patient overall survival similarly to O6-methylguanine-DNA methyltransferase (MGMT) promoter methylation and may aid in predictions in gliomas with mismatch-repair variants of unknown significance, where MGMT is not predictive. Our findings suggest that cell mass is a promising functional biomarker for cancers and drugs that lack genomic biomarkers.

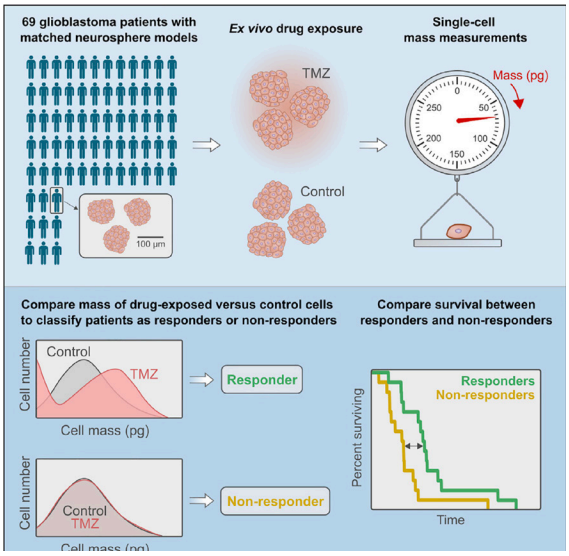

▲Figure 1: In a retrospective study, func-tional drug susceptibility testing predicts the response of patients with glioblastoma to chemotherapy. By detecting subtle changes in tumor cell mass after ex vivo drug exposure, testing can predict treat-ment response with power comparable to the standard-of-care genomic biomarker.

FURTHER READING

- M. A. Stockslager, S. Malinowski, M. Touat, J. C. Yoon, J. Geduldig, M. Mirza, A. S. Kim, P. Y. Wen, K. H. Chow, K. L. Ligon, and S. R. Manalis, "Functional Drug Susceptibility Testing Using Single-cell Mass Predicts Treatment Outcome in Patient-derived cancer Spheroid Models," *Cell Reports*, vol. 37, no. 1, 2021.

Thermally Drawn Piezoelectric Fiber Enables Fabric for Acoustic Healthcare Monitoring

G. Noel, W. Yan, E. Meiklejohn, G. Rui, L. Zhu, Y. Fink
Sponsorship: NSF Graduate Research Fellowship Grant No. 1745302.

Since the invention of the stethoscope, healthcare professionals have used acoustic signals to monitor patient health. Although the stethoscope is widely used, its form factor does not allow continuous monitoring, leaving much of the information from the acoustic signals of the body uncaptured. Here, we present a novel piezoelectric fiber microphone device that can be incorporated into fabrics to effectively detect sound. Using the thermal fiber-drawing technique, multiple viscoelastic materials flow in a laminar regime to produce a device with microscale features that maintain the same cross-sectional geometry as the macroscopic preform. The piezoelectric domain consists of poly(vinylidene fluoride-trifluoroethylene) and barium titanate nanoparticles; during the draw, cavities form between the polymer and the particle on either side of the particle in the direction of the draw, resulting in a novel ferroelectret material with a high piezoelectric coefficient. The fiber's shape and flexibility allow it to be woven into fabrics, and the sensitivity of these "acoustic fabrics" is comparable to that of handheld microphones. In clothing, the fibers reliably detect the heartbeat and breathing rate of the wearer. With further development, arrays of fibers can be used to continuously capture acoustic signals that provide the wearer with insight into their health, making healthcare more accessible outside clinical settings.

Fabrication of Transparent Displays for Wearable Electronic Biomonitors

S. Payra*, S. Ben-David*, C. Gregory*, R. Brenes, R. Ram, F. Niroui
*Contributed equally
Sponsorship: MIT Department of Electrical Engineering and Computer Science, 6.s059 Class

While advances in polymeric materials have enabled the creation of flexible biosensors, there has been limited progress on transparent "electronic skins" that allow wearers to view, monitor, and interact with their biological data. Towards this objective, in this work we present a candidate thin-film organic light-emitting diode (OLED) composition that we utilize to fabricate seven-segment displays upon transparent glass substrates. We compare MEH-PPV and Alq_3 emitting layers and then create, connect, and encapsulate multiple Alq3-based OLED displays using a stackup of {ITO/MoO_3/NPB/Alq_3/LiF/Al}. Spring-loaded pins are used to interface with two devices, and display circuitry is designed with a 9V LED drive level / 3V logic level using a back-to-back n-channel enhancement metal-oxide-semiconductor field-effect transistor (MOSFET) architecture. When interfaced with a microcontroller and temperature sensor, this prototype can display body temperature on the nanofabricated OLED displays. The techniques utilized present a basis upon which to develop wearable biomonitors that measure and display biometric data. Future development will aim at adapting these processes to polymer substrates for the creation of flexible wearable devices that can seamlessly integrate into garments or onto wearers' skin.

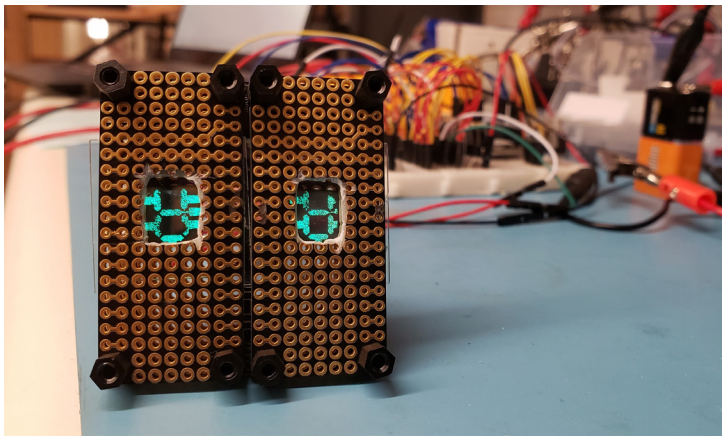

▲ Figure 1: Photograph of the fabricated seven-segment displays connected to a temperature sensor for temperature readout.

Navigational Chemistry for Self-Editing or "Lamarckian" Genomes and Targeted Drug Delivery Using a Bio/Nano TERCOM Approach

J. M. Protz
Sponsorship: Protz Lab Group; BioMolecular Nanodevices, LLC d.b.a. Ariadna

Navigational chemistry has been actively studed by the investigator for two decades. The work described here is focused on developing cells or cell-free reactions that estimate their location by correlating the evolution of their sensed fluid environment (e.g ., temp., salinity, sugar, pH, ion conc., etc.) against an embodied map and then self-edit the content of their genomes in a way that depends on said estimate. Editing the genome shifts the expressed phenotype and the heritable genotype . The laboratory component has been focused on preparing and testing a liposome-encapsulable mixture of oligo-modified ribonucleaic acid (RNA) and nucleases that yields path-dependent doses of therapeutic RNA while en route to a target site. This is the key element of an envisioned self-editing genome reaction chain. In this chain, a read-only "junk DNA" segment of a plasmid would transcribe into RNA strands having a spectrum of coding heads and consumable tails. The tails would be attacked by an exonuclease sensitive to substrate and local environment, causing the tails to function as path-sensitive fuses and the spectrum of the surviving RNA to depend on path. The surviving RNA would be reverse-transcribed into DNA and integrated as expressible genes in a read-write portion of the plasmid, with concurrent random erasures keeping plasmid length roughly constant. By this process, the genetic composition of the read-write region would evolve with changing environmental paths . A related effort led by the investigator explores drug delivery using particles that exhibit path-dependent doses or conformation. Both are related to terrain contour matching (TERCOM), a technique used in air navigation, and both build on prior study by the investigator and his group of nanoparticles that record the trajectory of their environment. Progress might enable new pharmaceuticals or the engineering of organisms that exhibit Lamarckian evolution or gene therapies that confer this ability.

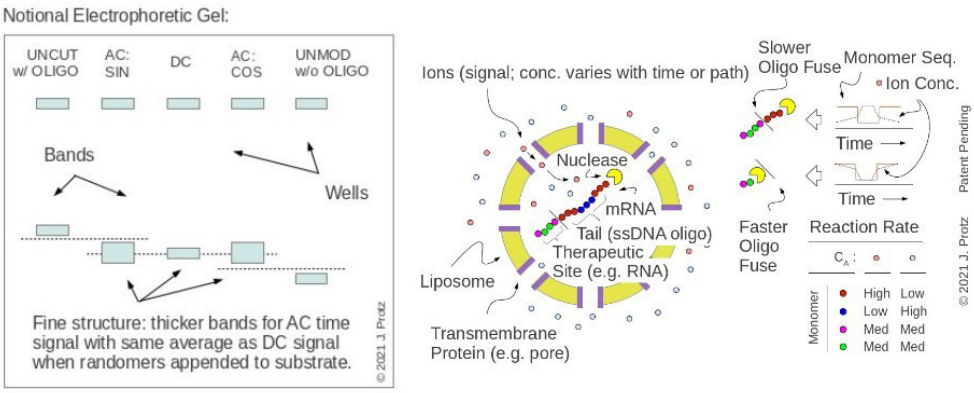

▲ Figure 1: (right) Nuclease with environmental and substrate sensitivity consumes tails faster when environmental path and tail sequence are better correlated; (left) if a mix of random tails is used, electrophoretic gel should exhibit fine structure in bands due to varying correlations between tail sequences and environmental paths, causing yielded strand length to vary.

FURTHER READING

- J. Protz, "Self-Editing or "Lamarckian" Genome using Bio/Nano TERCOM Approach," MIT, Cambridge, MA, *MTL Annual Research Report*, p. 13, 2021.
- J. Protz, "Methods and Compositions for Targeted Delivery, Release, and/or Activity," *Int'l. Patent App.* PCT/US2021/016111, 1 Feb 2021. See also Int'l. Patent App. PCT/US2019/031395 (WO/2019/217601), 8 May 2019.
- J. Protz, A. Lee, A. Jain, M. Slowe, E. Vasievich, and T. LaBean, "Bio-Nano TERCOM for Drug Delivery Using Oligos, RNA, and Nuclease," Proc. MIT *MTL Annual Research Conference (MARC 2022)*, S7.05, pp, 25-26, 2022.

Adaptable Engineering of Cellulose-based Vertical Flow Assays for Rapid Diagnostics–The Case of COVID-19

D. M. Y. Tay, S. Kim, E. H. Yee, E. A. Miller, K. J. Sung, Y. Hao, H. D. Sikes
Sponsorship: Deshpande Center for Technological Innovation, NIH Rapid Acceleration of Diagnostics (RADx) program, 3M Company, Quanterix Corporation, Singapore's National Research Foundation

Rapid diagnostic tests (RDTs) are integral to effective disease response and control. To maximize their potential for population-wide epidemiological control, accessibility and widespread use are two key factors. The commonplace lateral flow assays (LFAs) are heavily reliant on nitrocellulose, of which supply can be strained in times of high demand such as during the ongoing COVID-19 pandemic, and also require processing prior to reagent immobilization. These features hamper the necessary large-scale distribution of RDTs. Here, we seek to overcome this limitation by enabling swift and efficient production of cellulose-based paper assays that do not depend on nitrocellulose and require minimal substrate processing. We accomplished this through the engineering of cellulose-binding domain onto binding proteins for rapid immobilization on cellulose. We subsequently demonstrate good clinical and lab-based performance for two orthogonal assay types: serological and antigen rapid tests and their compatibility with roll-to-roll mass manufacturing. Specifically, we were able to detect antibodies present in human serum towards the severe acute respiratory syndrome coronavirus 2 (SARS-CoV-2) nucleocapsid (N) protein, as well as SARS-CoV-2 (N) protein in saliva and swab samples using modified versions of the cellulose-based vertical flow assays (VFAs). Both saliva and swab samples achieve clinically relevant detection ranges appropriate to probe the serological status and viral loads of patients, respectively. We envision that our proposed workflow has the capacity to be implemented in response to immense RDT demands in future pandemics and pave the way to newer and exciting innovations in paper-based assays.

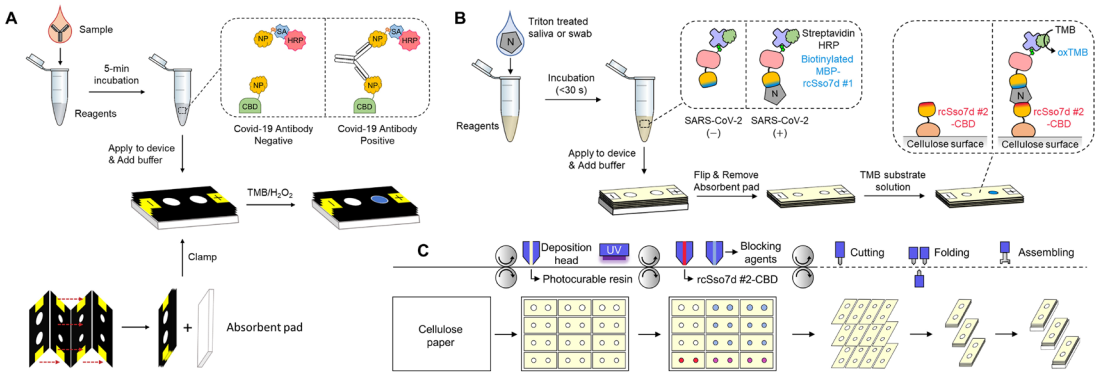

▲ Figure 1: Production and assay workflow of cellulose-based VFAs. (A) Serological assay for SARS-CoV-2 antibodies in human serum. (B) Rapid antigen test for SARS-CoV-2 N protein. (C) Schematic of large-scale manufacture of VFAs.

FURTHER READING

- Kim et al., *ACS Sens.*, vol. 6, p. 1891, 2021.
- Kim et al., *ACS Appl. Mater. Interfaces*, vol. 13, p. 33, 2021.
- Jia et al. *Lab Chip*, vol. 22, no. 7, p. 1321, 2022.

Femtomolar Detection of SARS-CoV-2 via Peptide Beacons Integrated on a Miniaturized TIRF Microscope

S. P. Tripathy, M. Ponnapati, S. Bhat, J. Jacobson, P. Chatterjee
Sponsorship: MIT Media Lab, MIT Center for Bits and Atoms, Jeremy and Joyce Wertheimer

The novel severe acute respiratory syndrome coronavirus 2 (SARS-CoV-2) continues to pose a significant global health threat. Along with vaccines and targeted therapeutics, there is a critical need for rapid diagnostic solutions. The most widely employed diagnostic tests for SARS-CoV-2 are reverse transcription-polymerase chain reaction (RT-PCR)-based methods, though other technologies based on clustered regularly interspaced short palindromic repeats (CRISPR) and loop-mediated amplification have been deployed as well. The best-in-class FDA-authorized diagnostics, such as RT-PCR, have limits of detection (LoD) of 10^2-10^3 ribonucleic acid (RNA) copies/ml, which is about 1-10 attomolar (aM) RNA in the test volume. RT-PCR tests, however, require laborious and expensive nucleic acid isolation, purification, and processing steps, which increases both the turnaround time of detection and the cost of testing. Alternatively, there are Food and Drug Administration- (FDA-)authorized low-sensitivity, inexpensive, and rapid diagnostics. These tests, which often rely on antigen detection, have limit of detection (LoD) of 10^5-10^7 RNA copies/ml, or around 1-100 femtomolar (fM). Recently, there has been a significant effort to detect SARS-CoV-2 via fluorescence-based readouts to allow for specific signal amplification. Such methods largely rely on binding to SARS-CoV-2 RNA or deoxyribonucleic acid (DNA), which requires isolation of nucleic acids, as described above.

In this work, we utilize computational protein modeling tools to suggest molecular beacon architectures that function as conformational switches for high sensitivity detection of the SARS-CoV-2 spike protein receptor-binding domain (S-RBD). Next, adopting the technology of total internal reflection fluorescence (TIRF) microscopy, we fabricate a miniaturized TIRF (mini-TIRF) microscope for seamless detection of peptide beacon activity in response to viral presence, enabling rapid and highly-sensitive detection of SARS-CoV-2. Integrating these beacons on a mini-TIRF microscope, we detect the S-RBD and pseudotyped SARS-CoV-2 with limits of detection in the femtomolar range. We envision that our designed mini-TIRF platform will serve as a robust platform for point-of-care diagnostics for SARS-CoV-2 and future viral threats.

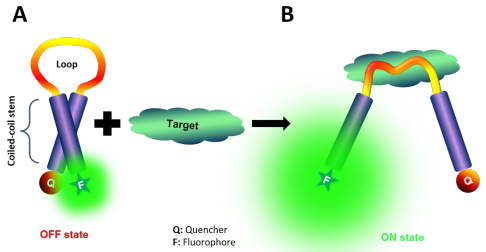

▲Figure 1: Schematic of pep-tide beacon architecture. A) Low-fluorescent state is closed heterodimer state of peptide beacon in absence of S-RBD. B) High-fluorescent state is open-coil state after binding of S-RBD with loop of peptide beacon.

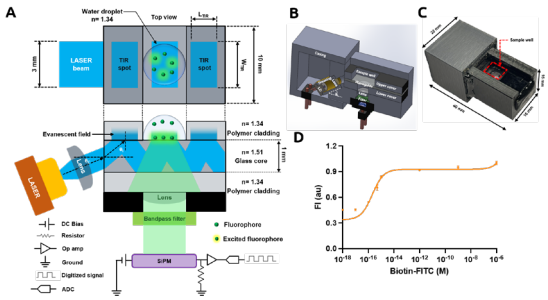

▲Figure 2: Design of mini-TIRF. A) Schematic showing engineering of mini-TIRF device. B) Internal architecture of cartridge shown in sliced solid work model. C) 3D printed cartridge containing laser diode, planar waveguide, collimating lens, optical filter, and SIPM. D) Detection of biotinylated FITC in 1X PBS, pH 7.4 from attomolar to micromolar concentration using mini-TIRF. LoD is defined as signal measured as three times standard deviation of baseline signal.

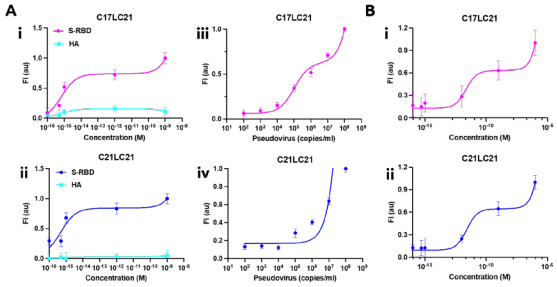

▲Figure 3: Detection of S-RBD and pseudotyped SARS-CoV-2 virus particles on mini-TIRF. A) Detection of recombinant S-RBD and Influenza H3N2 (HA) in 1X PBS by HPLC-purified i) C17LC21 (n=5), ii) C21LC21 (n=5) immobilized on mini-TIRF. Detection of SARS-CoV-2 spike protein bearing pseudovirus by HPLC-purified iii) C17LC21 (n=5), iv) C21LC21 (n=5) immobilized on mini-TIRF. B) Detection of recombinant S-RBD in human saliva sample by HPLC-purified i) C17LC21 (n=3), ii) C21LC21 (n=3) immobilized on mini-TIRF.

FURTHER READING

- C. Mueller and T. N. Grossmann, "Coiled-coil Peptide Beacon: A Tunable Conformational Switch for Protein Detection," *Angewandte Chemie International Edition*, vol. 57, pp. 17079-17083, 2018.
- S. Ramachandran, D. A. Cohen, A. P. Quist, and R. Lal, "High Performance, LED-powered, Waveguide Based Total Internal Reflection Microscopy," *Scientific Reports*, vol. 3, pp. 1–7, 2013.

Highly Tunable, Rapid Manufacturing of Microneedles for Controlled Vaccine Delivery Applications using Multiphoton 3D Printing

D. Varshney, J. Han, J. L. Daristotle, I. Sadeghi, M. Kanelli, R. S. Langer, A. Jaklenec
Sponsorship: Bill and Melinda Gates Foundation (INV-007842)

Rationally designed microneedle drug delivery systems enable precise spatiotemporal control of vaccination. Standard manufacturing processes such as computer numerical controlled (CNC) machining and photolithography are prerequisites for fabricating such delivery devices. However, due to tolerance limitations and lengthy production times, the manufacturing of microneedle patches is inherently restricted by feature size and subject to production inefficiency. In this work, multiphoton 3D printing (MPP) was used to rapidly prototype and develop microneedles varying in size and shape for enhanced vaccination. We report the effect of various printing parameters on feature resolution and printing time. High-resolution MPP enables production scalability and antigen-specific device customizability, where parameters such as needle pitch, patch size, and tip-angle can highly influence vaccine efficacy. Such devices may be critical for rapid response to disease outbreak in future applications.

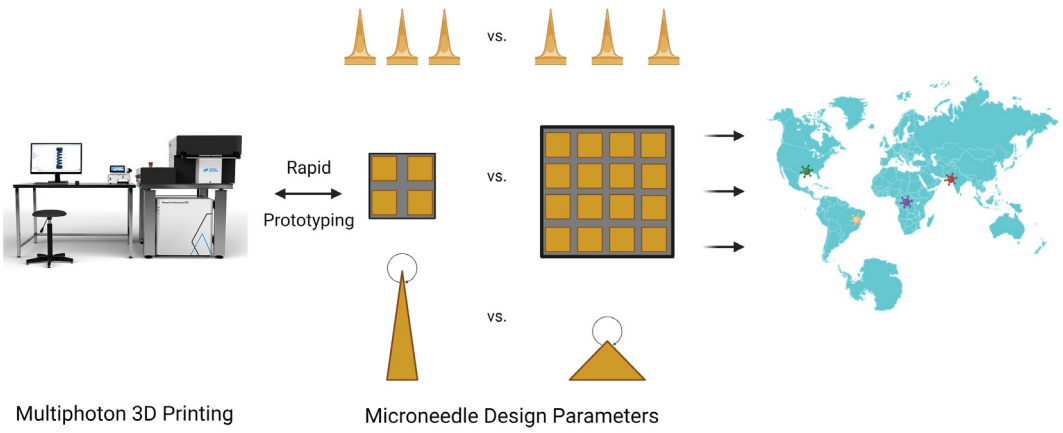

▲ Figure 1: Microneedles manufactured via multiphoton 3D printing enables rapid, customizable, and spatiotemporally controlled vaccination response to global disease outbreak.

Characterization of 3D-printed, Tunable, Lab-grown Plant Materials

A. L. Beckwith, J. Borenstein, L. F. Velásquez-García
Sponsorship: Draper Laboratory

Wood has traditionally been viewed as a low-cost, widespread commodity. However, current practices for wood procurement are unsustainable. Wood supply is increasingly strained, and, in many ways, trees are non-ideal to produce wood: they are affected by climate, seasons, and producing a small fraction of wood from the total mass of the tree.

We recently pioneered an approach to generate plant-based materials in vitro without needing to harvest or process whole plants, making possible the high-density production of plant-based materials unaffected by such constraints. In addition, the process is compatible with additive manufacturing. We now report the first physical, mechanical, and microstructural characterization of plant materials generated with Zinnia elegans cell cultures using such methodology. The results show that the properties of the plant materials vary significantly with adjustments to hormone levels present in growth medium. In addition, the data show that the use of bioprinting and casting enables the production of net-shape objects in forms and scales that do not arise naturally in whole plants (Figure 1). Further work could entail the development of processes for other plant species and/or producing other biopolymers.

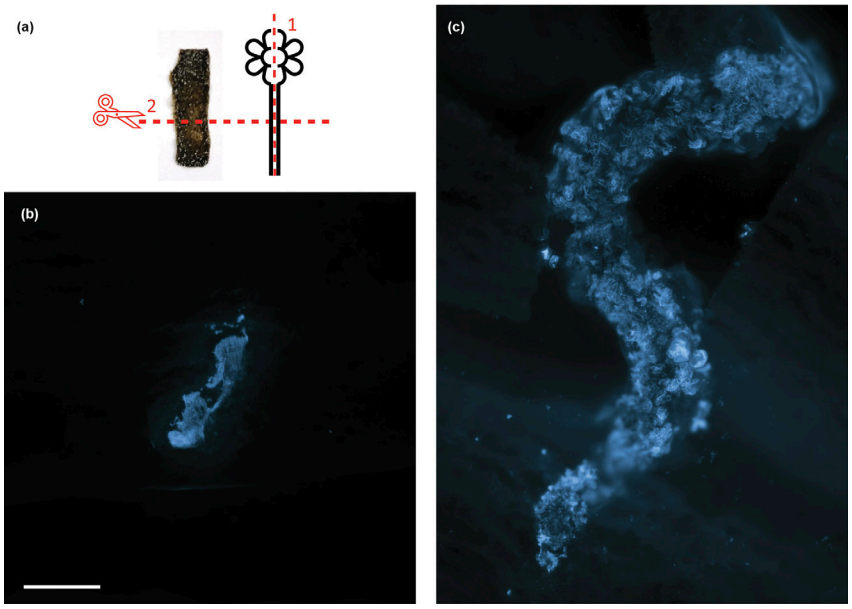

▲Figure 1: (a) Stem samples were halved lengthwise (cut 1) and dried before fixing in wax and sectioning with a microtome along cut 2. (b) Cross-section of a halved and dried Zinnia stem. (c) Cross-section of a grown material sample sliced along the shortest dimension, greatly surpassing the size of the stem, even though they have the same age. Scale bar equals 500 micrometers. From A. Beckwith et al., Materials Today (2022).

FURTHER READING

- A. Beckwith, J. Borenstein, and L. F. Velásquez-García, "Physical, Mechanical, and Micro-structural Characterization of Novel, 3D-printable, Tunable, Lab-grown Plant Materials Generated from Zinnia Elegans Cell Cultures," *Materials Today*, vol. 54, pp. 28 – 41, April 2022. DOI: https://doi.org/10.1016/j.mattod.2022.02.012
- A. L. Beckwith, J. Borenstein, and L. F. Velásquez-García, "Tunable, Plant-based Biomaterials via In Vitro Cell Culture Using a Zinnia Elegans Model," *Journal of Cleaner Production*, vol. 288, p. 125571, Mar. 2021. DOI: https://doi.org/10.1016/j.jclepro.2020.125571
- Z. Sun and L. F. Velásquez-García, "Monolithic, FFF Printed, Biodegradable, Biocompatible, Dielectric–conductive Microsystems," *Journal of Microelectromechanical Systems*, vol. 26, no. 6, pp. 1356 – 1370, Dec. 2017. DOI: https://doi.org/10.1109/JMEMS.2017.2746627

Absolute Blood Pressure Measurement using Machine Learning Algorithms on Ultrasound- based Signals

H. Wang, A. Chandrasekhar, J. Seo, A. Aguirre, S. Han, C. G. Sodini, H.-S. Lee
Sponsorship: MIT J-Clinic, Philips, Analog Devices, MIT-IBM Watson AI Lab, NSF CAREER Award

In an intensive care unit (ICU), physicians can use an invasive arterial catheter to measure the blood pressure (BP) waveform with high resolution. In non-ICU settings, arterial catheters are not used, and clinicians must rely upon isolated spot measurements from a non-invasive arm-cuff device that cannot measure the absolute BP waveform. In this project, we are developing an algorithm to convert data from an ultrasound-based device to absolute BP waveforms. Such a device may offer a quantitative method to perform rapid hemodynamic profiling of patients in an emergency room, step down clinical ward, or outpatient clinic who cannot undergo invasive BP measurements.

We propose a non-invasive way to get BP waveform with blood flow velocity and arterial area obtained from non-invasive ultrasound signals (Figure 1a). One key drawback of the ultrasound-based device is that the output BP waveform has an arbitrary reference, so we have to estimate the mean arterial pressure (MAP) and leverage transmission line model to calculate the absolute BP value. Hence, we propose to use a machine learning model containing transformer encoder layers to regress the MAP accurately. The input features are flow velocity and the shape of BP waveform. Since the number of subjects is limited in the training set, we propose to use contrastive loss to guide the feature extraction and improve generalization. The contrastive loss encourages the features of beats of the same subject to be similar. When we enlarge the contrastive loss , the feature vector will be trained to contain as little subject-specific information as possible. Therefore, the model can generalize better to unseen subjects. On a collected dataset, the proposed method improves the MAP error standard deviation from baseline 10.6 mmHg (only training the MAP regressor) to 9.2 mmHg. Our algorithm has large potential to make affordable BP measurements accessible to everyone.

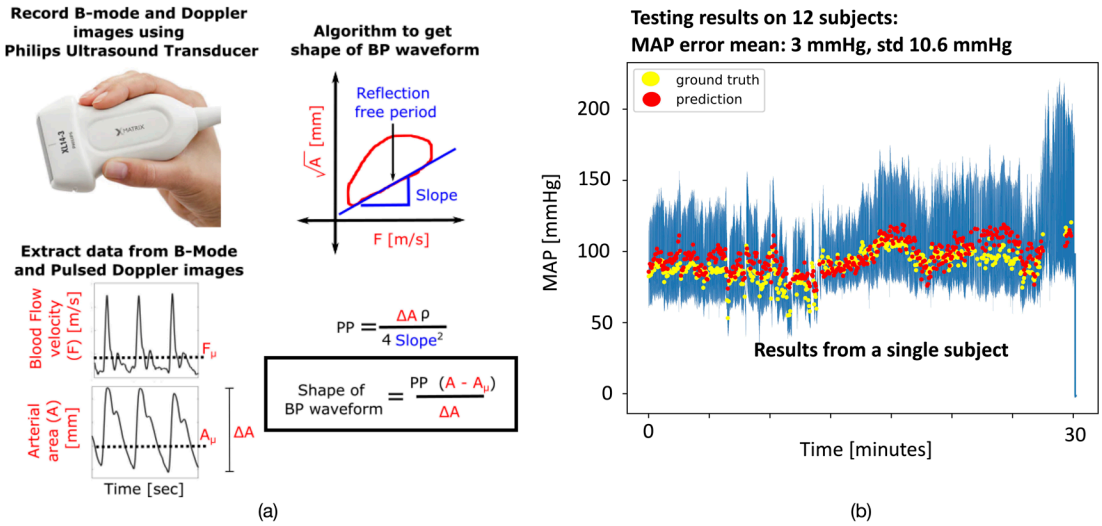

▲ Figure 1: (a) The whole pipeline of using machine learning-based algorithms to get BP waveforms from ultrasound data, and (b) MAP prediction results for a single subject.

FURTHER READING

- V. Novak, and L. Mendez, "Cerebral Vasoregulation in Diabetes" (version 1.0.0), *PhysioNet*, 2020. https://doi.org/10.13026/m40k-4758.

Electrokinetic-based Biomolecule Separation Technology

E. Wynne, J. Prince, C. Long, M. Cui, H. J. Kwon, J. Han
Sponsorship: Federal Drug Administration, SMART CAMP

Contamination of pharmaceutical products by viral and bacterial adventitious agents pose challenges to the safety and cost of a biomanufacturing process. Rapid detection of low abundance contaminants from a large volume requires concentrating the relevant biomolecules into a smaller volume that is compatible with sensitive downstream detection methods.

Electrokinetic (EK) concentration technology uses ion exchange membranes to selectively remove ionic species from a microchannel. When a voltage bias is applied to an EK concentrator, charged biomolecules become trapped by the increased electric field in the ion depletion region.

Recently significant progress has been made in constructing EK concentrators from inexpensive materials that are more compatible with large-scale manufacturing. See figures A and B.

Numerical simulation work is being used to better comprehend the non-linear electroosmotic flow present in these large-scale EK concentrators; an example is seen in Figure (C). Increasingly complex devices have many parameters that can affect performance such as applied voltage, flow rate, and channel dimensions. These simulations could help to find ideal operating parameters.

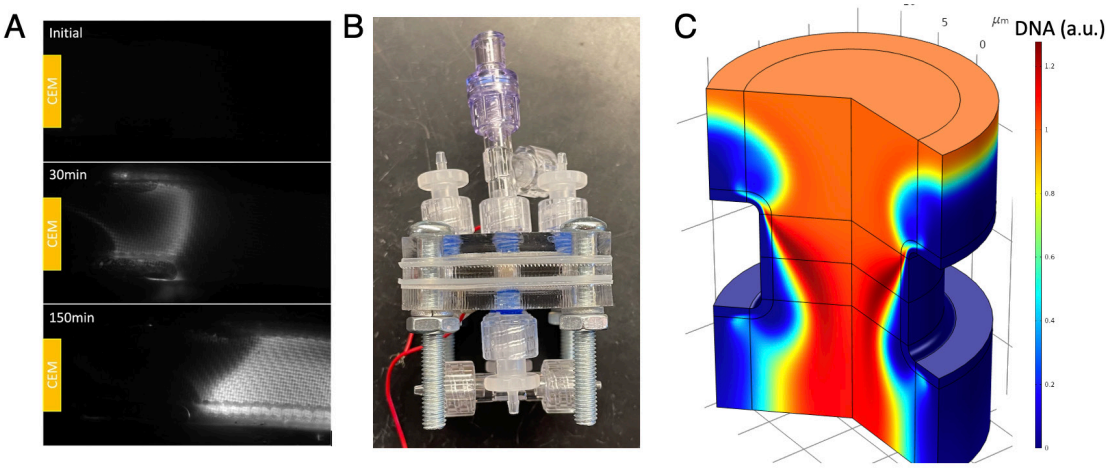

▲ Figure 1: (A) shows accumulation of fluorescently tagged DNA in an EK concentrator constructed using plastic channels and mesh. Additionally, (B) shows a high-throughput device made entirely from plastic that can enrich viruses from several milliliters of solution per hour into a volume as small as 200 microliters. (C) An example of numerical simulation work being used to better comprehend the non-linear electroosmotic flow present in these large-scale EK concentrators.

Minimally Invasive Wireless Stimulation of the Brain

S. Yadav, D. Sarkar
Sponsorship: NIH, Media Lab Consortium

Clinically, neural-stimulation finds application for treatment of neurological diseases like Parkinson's, Alzheimer's, etc. Currently, non-genetic neural stimulation faces challenges that can be classified into two broad categories: (a) tethered but requires invasive surgery (examples include electrodes, multi-electrode arrays, etc.) and (b) untethered but lacks cellular precision (examples include transcranial direct current stimulation, transcranial magnetic stimulation, etc.). Further, modalities that lie in between these two in terms of invasiveness involve implantation of devices inside the brain tissue and can be wirelessly actuated using fields which can be acoustic, magnetic, and electromagnetic, including radio frequency and light. Currently all these technologies are either invasive or cannot achieve spatio-temporally precise stimulation. To solve these challenges, we need to have a technology that qualifies on the following criteria: untethered remotely controlled devices to achieve minimal invasiveness and micron-sized to achieve single cell stimulation with minimal tissue displacement.

To achieve untethered neuron stimulation with single-cell resolution, we have developed photovoltaic arrays that can be wirelessly actuated with light to achieve spatiotemporally precise stimulation with single neuron resolution. These devices are based on organic polymers to operate at selective wavelengths. The chosen device structure is essentially a vertical stack of three components–anode, organic polymer, and cathode–fabricated on a silicon substrate. The choice of electrodes is based on the required built-in electric-field, transparency, and the charge injection capacity. Currently, we are carrying out in-vivo work for wireless stimulation of the brain in rodent models.

An Implantable Piezoelectric Microphone for Cochlear Implants

A. Yeiser, J. Zhang, L. Graf, C. McHugh, K. Broderick, J. Kymissis, E. Olson, H. H. Nakajima, J. H. Lang
Sponsorship: NIH Grant (R01DC016874)

Cochlear implants (CIs) are arguably the most successful sensory implant, with over 700,000 implanted up to 2019. Modern cochlear implants rely on external microphones. While these microphones are quite sensitive, they impose lifestyle restrictions on CI users and cannot replicate the sound localization cues from the shape of the outer ear. The development of a practical implantable microphone is a decades-old problem without good solutions. We think our implantable piezoelectric microphone design makes promising inroads towards this goal.

Our microphone design, shown in Figure 1, is a triangular piezoelectric cantilever about 3 mm long and 3 mm wide at the base. The cantilever consists of two layers of the piezoelectric polymer polyvinylidene difluoride (PVDF) sandwiching a flex printed circuit board, with charge sense electrodes at the layer interface providing a shielded differential output. The tip of the cantilever rests on the umbo—the point of the cone-shaped eardrum and detects audio-frequency displacement as low as 15 picometers when connected to our custom-built differential charge amplifier. When tested in a cadaveric human temporal bone as shown in Figure 2, the cantilever achieved sensitivity comparable to a good hearing aid microphone, with equivalent input noise (EIN) comparison shown in Figure 3.

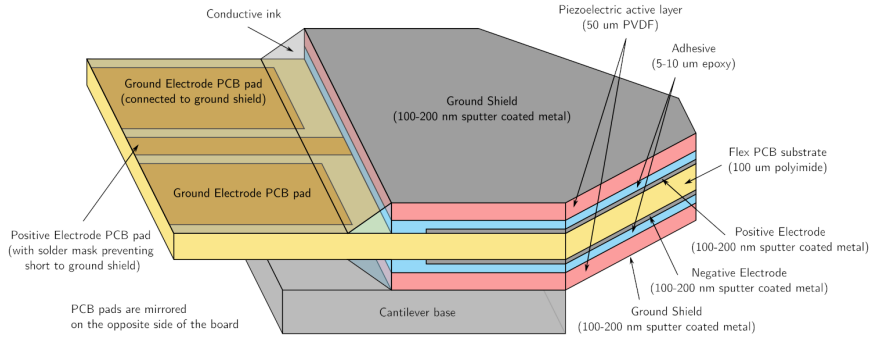

◀ Figure 1: PVDF microphone stackup, showing, showing charge-sense electrodes capacitively coupled to the PVDF through a thin glue layer.

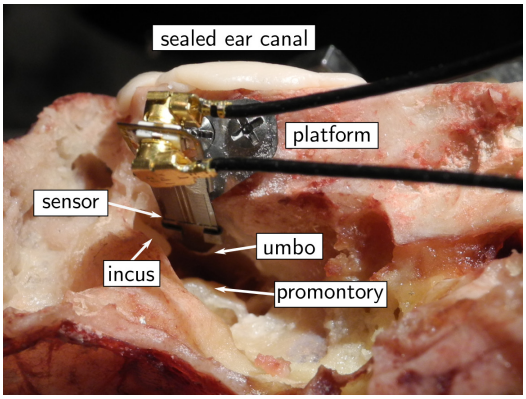

▲ Figure 2: Testing the cantilever-mic in a human temporal bone. The microphone rests on the umbo.

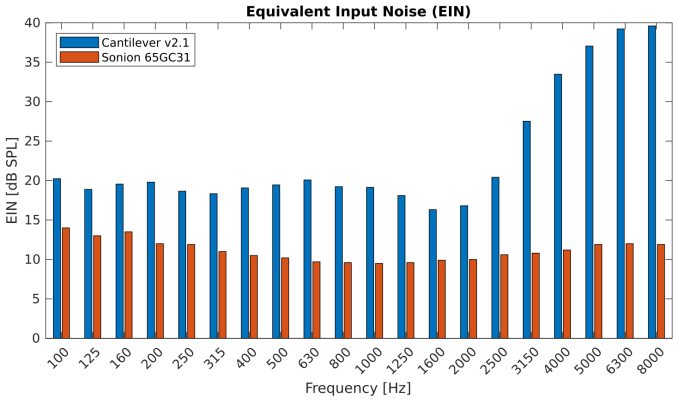

▲ Figure 3: Implanted cantilever EIN vs. a Sonion 65GC31 electret hearing aid microphone.

FURTHER READING

- D. Calero, S. Paul, A. Gesing, F. Alves, and J. A. Cordioli, "A Technical Review and Evaluation of Implantable Sensors for Hearing Devices," *BioMedical Engineering Online*, vol. 17, no. 1, p. 23, Dec. 2018.